

An approach to understand stamping force behavior that enables the quantification of resistive force considering drawbead geometry and BHF intensity

Alex Raimundo de Oliveira¹, Chetan Nikhare², Ravilson Antonio Chemin Filho¹
and Paulo Victor Prestes Marcondes¹

¹Mechanical Engineering Department, Federal University of Paraná, PR, Brazil

²Mechanical Engineering Department, The Pennsylvania State University, Erie, PA, United States

***Corresponding author email address:** cpn10@psu.edu

Summary: The manufacturing of automotive bodywork for most vehicle models is predominantly carried out through the process of sheet metal forming, which stands out for its efficiency in meeting the high demand of the automotive industry. However, this segment faces increasing challenges related to productivity, structural design, mechanical performance, and vehicle safety, in addition to the requirements brought by automotive electrification, which impose the adaptation of materials and construction solutions. In this context, several research efforts have been conducted focusing on the modernization of body structures, involving the development of new steel alloys, process improvements, and the adoption of innovative designs. One such development is the application of a system for measuring the resistive force exerted on metal sheets during the modified Nakazima stamping test. Unlike the traditional method, the study incorporates additional variables such as Blank Holder Force (BHF) and drawbead geometry (DB), aiming to provide a more precise analysis of the formability of Advanced High-Strength Steels (AHSS). Samples with dimensions of 200 × 200 mm were used, where resistive forces resulting from the interaction between the tooling and the metal sheet were recorded. The developed system enabled the identification of force behavior in distinct regions of the part—flange, die radius, and punch pole—allowing for the quantification of resistive force as a function of DB geometry and BHF intensity. The results highlight the significant impact of these variables on the performance of the forming process, contributing to a better understanding of the mechanical behavior of materials and the optimization of solutions in the context of automotive engineering.

Keywords: Forming Limit Curve, Formability, Grid Analyses, Concentric circles method, Nakazima Test, Drawbead.

1. INTRODUCTION

The manufacturing of automotive body structures involves the production of components with complex geometries, requiring detailed and precise engineering design in the development of stamping tools. To ensure quality and efficiency in production, it is essential to consider a series of process parameters that affect the formability of materials, directly influencing the performance of the process and the sheet metal conformability. In order to meet the automotive industry's demand for lighter and safer vehicles, the steel industry has been challenged to develop new steel alloys with mechanical properties that enable high strength and ductility—essential for ensuring structural integrity during manufacturing processes, especially in the formation of complex parts.

The manufacturing process of formed components, particularly in the automotive sector, depends crucially on stamping tools, or dies, which ensure product quality. Researchers have focused on improving tools, seeking solutions that result in high-quality products and reduced tryout time (tool adjustments and

testing). These investigations involve a detailed analysis of process variables such as stamping speed, applied force, temperature, and lubrication—factors that, when optimized, increase efficiency and precision, resulting in components with better finishes and shorter production times.

The Forming Limit Curve (FLC), initially proposed by Keeler (1965) [1], Goodwin (1968) [2], and Woodthorpe et al. (1969) [3], remains an essential tool for predicting the formability limits of metal sheets. Its application allows for the anticipation of failures, such as cracks and fractures, before they occur during the forming process. The FLC is usually determined through the Nakazima test, standardized by ISO 12004-2 (2008) [4], which assesses the behavior of sheets under different deformation states, using specimens of varying widths onto which circular grids are imprinted for deformation monitoring.

Several studies employ tensile tests, digital image correlation (DIC), and finite element method (FEM)-based simulations to measure deformations in metal sheets and determine the FLC. These approaches combine high experimental precision with advanced computational modeling, enabling a deeper analysis of material mechanical behavior during forming processes. Works such as those by Schwindt et al. (2015) [5], Paul (2021) [6], Affronti and Merklein (2017) [7], Leonard et al. (2018) [8], Belloni et al. (2019) [9], Iquilio et al. (2019) [10], Górszczyk et al. (2019) [11], and Barlo et al. (2019) [12] highlight the importance of these methodologies in optimizing and evaluating industrial processes.

More recent studies, such as those by Hino et al. (2014) [13], Pan et al. (2014) [14], Cardoso et al. (2016) [15], Frohn-Sörensen et al. (2022) [16], Oliveira et al. (2022) [17], Sanrutsadakorn et al. (2023) [18], and Rezazadeh et al. (2024) [19], reinforce the relevance of FLC as a reference in the development and characterization of materials used in demanding industrial sectors, such as the automotive industry, which extensively employs advanced high-strength steels (AHSS).

Shen et al. (2022) [20] conducted a comparative analysis between high-manganese steel and DP1000 steel, highlighting the influence of microstructure and process conditions on fracture toughness and formability through the determination of Forming Limit Curves (FLC), experimentally validated via numerical simulations. Additionally, new methodological approaches are being proposed to expand the understanding of metal sheet formability under complex and nonlinear deformation conditions, as demonstrated by studies from Pereira et al. (2024) [21], Katiyar (2024) [22], and Park et al. (2024) [23]. These studies present more robust and precise models aimed at optimizing the design and manufacturing of automotive components, promoting greater structural efficiency and reliability in forming processes.

In recent years, the development of advanced high-strength steels (AHSS) has driven a significant transformation in industrial processes, particularly in automotive manufacturing. The introduction of these more complex alloys has imposed new requirements on forming parameters, making in-depth investigations essential to understand deformation mechanisms and the influence of stamping tools on material formability. Several studies have explored the use of dual-phase steels and alternative techniques to increase production efficiency and reduce costs, as demonstrated by Abeyrathna et al. (2015) [24], Ke et al. (2018) [25], Schmid et al. (2019) [26], Barlo et al. (2019) [12], and Sarand & Misirlioglu (2024) [27]. These works highlight the potential of these innovations to meet the growing demands of the automotive industry.

Welding, another widely applied process in this sector, has also been a subject of study, particularly regarding its influence on microstructure and mechanical properties of materials. Research by Khan et al. (2023) [28], Rajak et

al. (2023) [29], Cheng et al. (2024) [30], and Mansur et al. (2021) [31] evaluated hardness in the heat-affected zone (HAZ) of dual-phase steels subjected to laser welding. Park et al. (2024) [23], in turn, specifically investigated DP600 steel sheets and observed that even after welding, the strength and formability properties were maintained without compromising structural integrity. These findings reinforce the feasibility of laser welding for automotive applications that require high mechanical performance, precision, and reliability.

In the field of hardness analysis and plastic behavior, Tupalin et al. (2021) [32] investigated the effects of thickness on the hardening of 12Kh18N10T steel sheets. Through microhardness measurements along the thickness, they observed that hardness tends to be lower at the center of the material, indicating a heterogeneous distribution of stresses and phases—fundamental for understanding the mechanical performance of these alloys.

Microscopy has played a fundamental role in the detailed analysis of AHSS microstructures, such as DP600, DP780, and TRIP940 steels. Techniques like Light Optical Microscopy (LOM), Scanning Electron Microscopy (SEM), and Electron Backscatter Diffraction (EBSD) have been widely used to investigate the distribution and interaction of martensitic, bainitic, and ferritic phases. These techniques are essential for thermal treatment control and mechanical property evaluation. Studies such as those by Zhang et al. (2024) [33] and Sarand & Misirlioglu (2024) [27] reinforce the relevance of these tools for deformation modeling and understanding the mechanical response of materials during forming processes.

These studies demonstrate that the evolution of materials and automotive manufacturing processes is closely linked to mastering process parameters, microstructural characterization, and computational simulation. Such advancements not only expand scientific knowledge but also directly contribute to the development of safer, lighter, and more efficient solutions for the automotive sector.

One of the central topics in research on mechanical forming is the analysis of variables associated with stamping tools and their direct impact on the formability of metallic materials. Parameters such as blank holder force (BHF), deformation speed, and lubrication conditions have been widely investigated with the aim of optimizing the production process and ensuring the integrity of manufactured components. Studies such as those by Meng et al. (2014) [34], Folle & Schaeffer (2017) [35], Schmid et al. (2019) [26], Paul et al. (2021) [6], Oliveira et al. (2022) [17], and Votava et al. (2023) [36] show that proper parameterization of these variables significantly contributes to process performance, especially in demanding applications such as the automotive and aerospace industries.

In this context, the adjustment of thermal cycles is also essential. Lima et al. (2022) [37], for instance, proposed a new heat treatment cycle with optimized parameters to maximize bainite formation and reduce ferrite fraction, improving mechanical properties without significantly increasing costs. Additionally, Webber & Knezevic (2024) [38] correlated the local hardness of ferrite and martensite phases with the global tensile strength of DP and martensitic steels, with values ranging from 590 to 1180 MPa, providing insights for material selection based on performance in forming processes.

Precise modeling of mechanical behavior has also been improved through methods such as the one proposed by Pereira et al. (2020) [39], who used hydraulic circular and elliptical expansion tests combined with simulation in the DD3IMP software, optimizing anisotropy and hardening parameters with the Levenberg-Marquardt method. Meanwhile, Trzepiecinski (2020) [40] developed an innovative experimental method for the incremental forming of AHSS steels,

combining controlled heating and finite element method (FEM) simulation, allowing for an integrated analysis of thermal and mechanical effects during the process.

During forming, particularly stamping, factors such as tools geometry, applied force, and deformation speed cause significant microstructural changes, such as work hardening. This phenomenon, directly related to increased material hardness, affects stampability and component integrity, especially in automotive applications. Recent research, such as that by Shen et al. (2022) [20], Lima T. et al. (2023) [41], Votava et al. (2023) [36], Sanrutsadakorn et al. (2023) [18], Nene (2024) [42], Rezazadeh et al. (2024) [19], and Sarand & Misirlioglu (2024) [27], identified a strong correlation between hardness variation and parameters such as drawbead geometry, lubrication, and process temperature.

In this same field, Zhang et al. (2024) [33] proposed a methodology based on experimental data and FEM simulation to accurately predict the behavior of anisotropic materials under large deformations. This approach proved effective for industrial forming processes, enabling improved structural performance of metallic components.

The role of experimental devices, such as the modified Nakazima test tooling, also stands out, as it can quantify resistive force during stamping and provide insights into deformation mechanisms. Tool instrumentation, as proposed by Oliveira et al. (2022) [17], allows real-time monitoring of the forces involved, contributing to the calibration of numerical models and validation of FEM simulations. This integration of tool design, simulation, and experimentation represents a significant advancement in forming engineering, directly impacting the reliability and efficiency of complex component manufacturing.

2. MATERIALS AND METHODS

The material used in this study was dual-phase steel 600 (DP600) with a thickness of 1.0 mm, supplied by Usiminas S/A. This material was chosen because it is an AHSS steel, increasingly replacing traditional HSLA steels in structural components of automotive bodies.

In this context, conducting studies focused on an in-depth analysis of the material's behavior during the stamping process proves not only feasible but also essential for advancing the understanding of forming mechanisms and improving applied techniques.

The mechanical properties and formability parameters were determined through tensile tests using the EMIC DL 3000 equipment. The specimens were manufactured in the machining laboratory of the Federal University of Paraná, following the ASTM E8/E8M (2016) standard. The fundamental mechanical properties of DP600 steel were obtained through tensile tests: Ultimate tensile strength (UTS), Yield strength (YS) and Total elongation (EL). Additionally, the formability parameters of the steel were evaluated: R-value (anisotropy factor) and n-value (strain hardening exponent).

These mechanical properties and formability parameters are essential for material characterization before stamping tests, verifying classification according to manufacturing standards, and determining mechanical properties that can be used as input in numerical simulation models.

Considering that this study focuses on a new analysis method, whose main variables are blank holder force (BHF) and drawbead geometry (DB), and given that the Forming Limit Curve (FLC) is an efficient parameter for quantifying the performance of stamping steels, the test configuration was as follows: The tests were limited to only four specimen dimensions, all 200 mm in length (Stretching

Region), with widths of 125, 150, 175, and 200 mm (see Figure 1). These specific geometries were chosen because they produce stretching deformations in the metal sheet, a condition where the effect of BHF and drawbead (DB) is predominant around the punch. Narrower specimens, whose sides do not directly contact the blank holder and thus generate deep drawing deformations, were excluded because they do not allow a precise evaluation of the BHF effect and DB geometry. It is worth noting that, in practical operations, the drawbead (DB) acts entirely around the piece's contour.

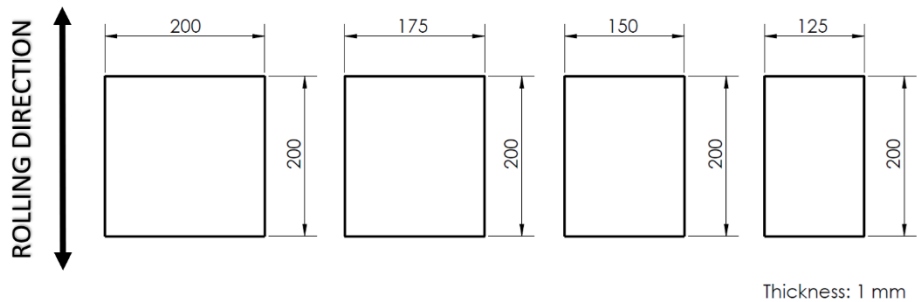


Figure 1 - Specimen's geometry carried out on Modified Nakazima's tests.

After the material was cut using a guillotine, the specimens were cleaned and printed with a circular grid of 5 mm in diameter using the screen-printing method. At this stage, the ink was prepared using a mixture of 90% epoxy paint and 10% nitric acid. This preparation ensured a good finish and strong adhesion of the ink to the specimen surface, providing the necessary conditions for measuring the planar deformations of the metal sheet using the printed circular grid.

The tooling used was the modified Nakazima test device, as proposed by Oliveira et al. (2022) [17], illustrated in Figure 2. In this test, the metal sheet was subjected to blank holder forces (BHF) of 785 kN and 1157 kN, with different drawbead (DB) geometries: flat (without teeth), circular, and square, as shown in Figure 3. Except for BHF and DB geometries, which were variables in the proposed tests, all other test parameters followed ISO 12004-2 (2008) [4].

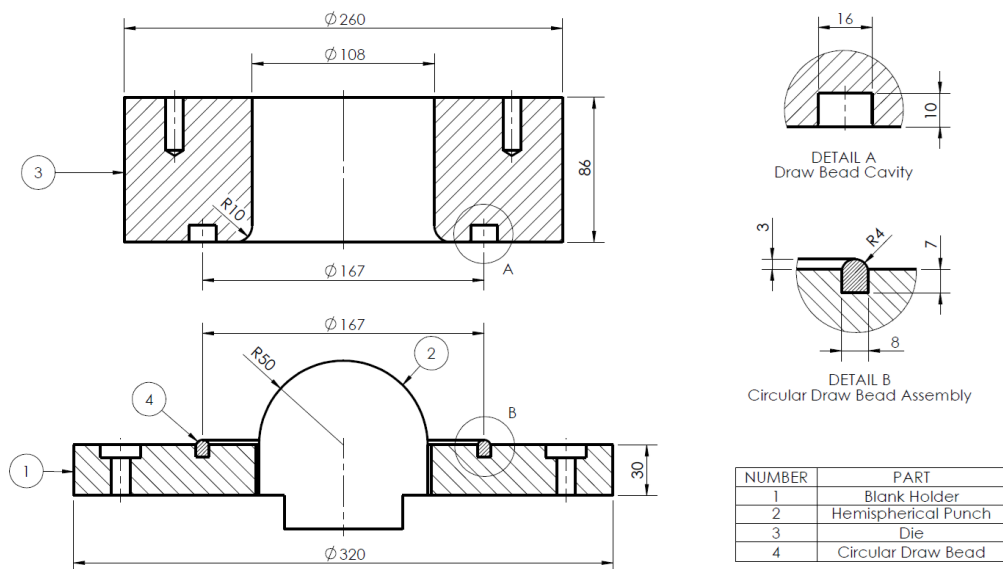


Figure 2 - Modified Nakazima test tool with interchangeable drawbead rings.

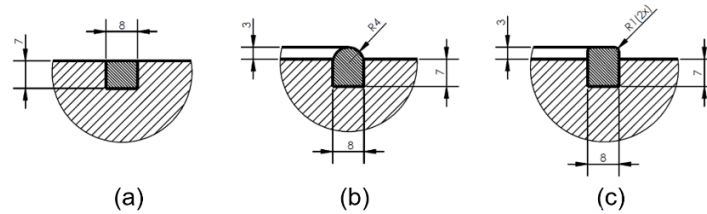


Figure 3 - Details and dimensions of the drawbead geometries: a) flat drawbead, b) circular drawbead and c) square drawbead. Oliveira et al. (2022) [17]

In addition to the grid mentioned above, concentric circles were printed on the top surface of the 200 × 200 mm specimens, covering the stamping regions (punch pole, die radius, and flange). This model was applied only to the 200 × 200 mm specimens, where the blank holder force (BHF) and drawbead (DB) acted uniformly around the entire contour of the samples.

The other specimens had less contact area with the blank holder in the width portion, where the sample dimension was smaller than the length, which consequently affected the deformation gradient of the material during stamping (non-uniform flow). The circles were manually drawn using a precision compass and permanent marking pens. The proposed diameters for the circles and the colors used for each analysis region are presented in Table 1.

Table 1 - Dimensions and regions of the concentric circles printed on the sheet metal surface. Red circles on the punch pole region, blue circles on the die radius region and black circles on the flange region.

Circles			DEFORMATION MEASUREMENT REGIONS
Regions	Diameter (mm)	Cor	
Punch pole (stamping)	25	Red	
	37.5		
	50		
	62.5		
	75		
	87.5		
Die radius	112	Blue	
	122		
	132		
Flange	144	Black	
	156		
	167		

The model proposed by Oliveira et al. (2025) [43] was originally developed for measuring deformations and microhardness in different regions of the stamped part, specifically in the flange, die radius, and punch pole, allowing for the creation of a variation profile of these properties along the specimen. In this study, however, the concentric circles were applied with the purpose of estimating the deformation forces acting in each stamping region, that is, between the regions delimited by these circles.

The deformation in each of the regions indicated in Figure 4 corresponds to the variation in the distance between the circles that define them. Only the deformation in region zero (0), at the punch pole, is calculated by the variation in

the diameter of the smallest circle (diameter of 25.0 mm). Thus, there is an initial distance (d_{0n}) between the circles defining each region, and after forming the sheet until rupture, the final distance (d_{fn}) for each region is measured. Measurements on the specimen are conducted along a straight line on the sheet, on the side opposite to the material fracture. Thus, the conventional deformation from region 1 to region 11 can be calculated using Equation (1):

$$e_n = d_{fn} - d_{0n} \quad (1)$$

While the true deformation is calculated using Equation (2):

$$\varepsilon_n = \ln(1 + e_n) \quad (2)$$

In the modified Nakazima test, the metal sheet flow during stamping is partially restricted by the action of blank holder force (BHF) and/or drawbead (DB). Despite this constraint, material slippage toward the die interior can occur, resulting in flow in the flange region. This displacement generates a containment force, known as resistive force, which can be measured. To quantify this resistive force, particularly in metal sheets used in the automotive industry, a measurement system was developed that simultaneously considers the influence of BHF and DB. This system allows for precise evaluation of the combined effect of these variables on the formability of advanced high-strength steels (AHSS), providing valuable insights for the optimization of forming processes and supplying relevant data for improving numerical simulation software. Figure 4 shows the developed system, which was adapted to the modified Nakazima test tooling, comprising a dynamometer with a load capacity of 500 kg.

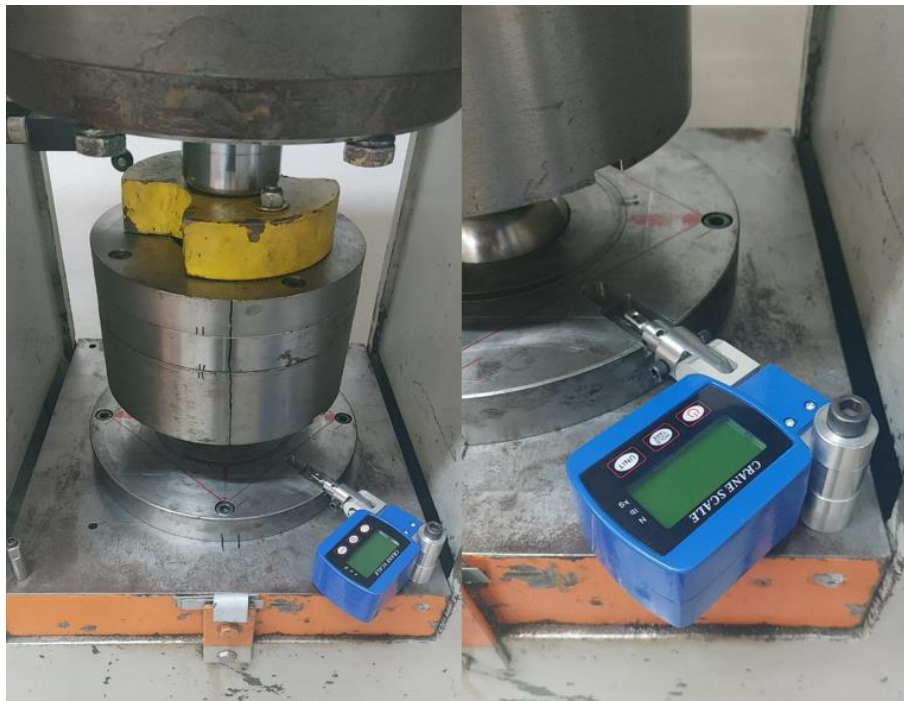


Figure 4 – Dynamometer for measuring the resistive force against sheet metal flow during stamping

3. RESULTS AND DISCUSSION

Table 2 shows the mechanical properties and stampability parameters of DP600 steel. Results obtained from uniaxial tensile tests in different positions in relation to the sheet rolling direction (0°, 45° and 90°).

Table 2 - Mechanical properties and stampability parameters of DP600 steel.

Dual Phase 600 Mechanical Properties					
Rolling direction	Total elongation (%)	Uniform elongation (Mpa)	Ultimate tensile strength (Mpa)	Strain hardening exponent (<i>n</i>)	exponent of plastic anisotropy (<i>r</i>)
0°	27.8	375.4	658.9	0.9937	2.255
45°	24.1	378.1	664.8	0.8752	0.217
90°	26.1	356.4	657.1	12.188	0.2201
Average	26	370	660.3	10.292	0.2209

According to the results in Table 2, the material used in this study demonstrated mechanical properties and stamping parameters consistent with expectations for DP600 steel. These findings align with the data reported by Barlo et al. (2019) [12], Khan et al. (2023) [28], Mansur et al. (2021) [31], Park et al. (2024) [23], and Chemin et al. (2013) [44]. The agreement among different studies reinforces the reliability of the material's characteristics and its performance under stamping conditions, validating its suitability for industrial applications.

Small variations in results between different batches of supplied sheets often indicate significant changes in stamping tests, due to the high sensitivity of this manufacturing process. Hence, it is necessary to conduct preliminary tests to characterize the materials received.

From the stamping tests, conducted until material rupture, a total of six FLCs were obtained for DP600 steel—one for each working condition, considering the two BHF values and the three DB geometries. Thus, the curves were grouped in a single graph, allowing a comparative analysis of the sheet formability under each test condition, as illustrated in Figure 5. It is important to highlight that the FLC results serve as a basis for identifying, based on the characteristics of the resistive force profile, the causes that led to better or worse material performance in each test configuration.

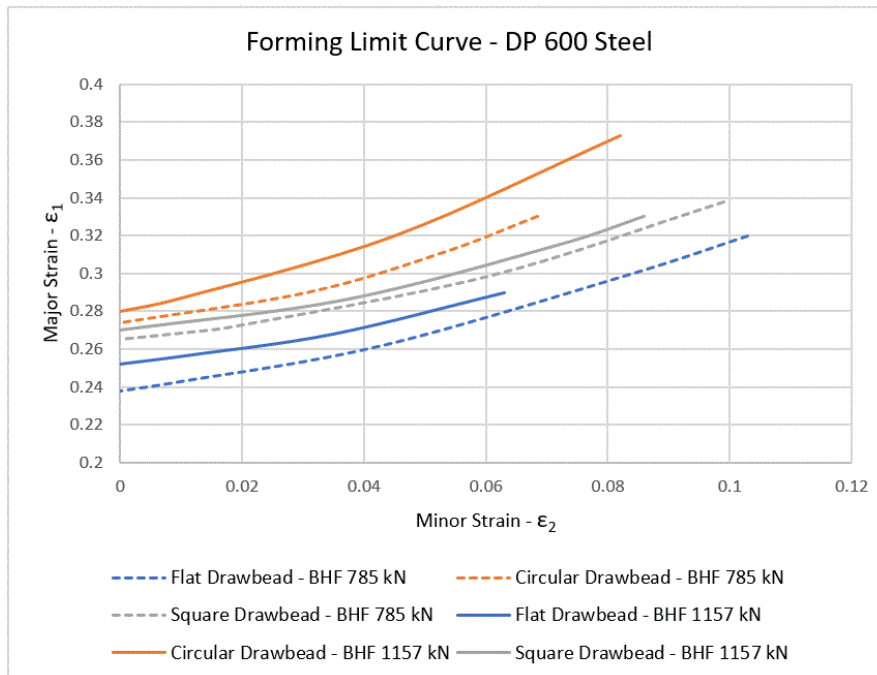


Figure 5 - Forming limit curves of DP 600 steel to different blankholder forces and drawbead geometries.

According to the presented forming limit curves (FLC), the best performance with the circular drawbead and the worst performance with the flat DB are evident for both applied blank holder forces (BHF). This result is very close to those presented by Oliveira et al. (2022) [17], who conducted similar tests on DP780 steel.

Another relevant finding is that, when analyzing each drawbead individually, all showed better performance with the BHF of 1157 kN, following the same results obtained by Chemin et al. (2013) [44], also for DP600 steel. These results once again prove that for very low BHF's, below a certain critical value, the sheet metal flow becomes too pronounced, compromising material formability. Thus, it can be affirmed that each DB has a very specific performance level, regardless of BHF. Although the circular DB with a BHF of 785 kN performs worse than with 1157 kN, it still outperforms the best performance of the square DB with 1157 kN. The same occurs when comparing the square DB with the flat DB, as the BHF of the square DB at 785 kN surpassed the best-performing FLC of the flat DB at 1157 kN.

In this way, the BHF clearly demonstrates the real gains in sheet metal formability through the use of DB, as well as how the application of a more suitable tooth geometry and BHF can further improve material formability. Considering these results, the detrimental effect of low restriction on material flow in the flange region on its formability becomes evident. The flat geometry, which restricts sheet flow less during stamping, produced lower BHF curves. Thus, the restrictive function of sheet flow, resulting from the use of DB and increased BHF, substantially improves the material's forming limit.

Through the analysis and discussion of results in this chapter, it was observed that the material's best performance, in terms of its forming limit, is achieved through a balance between BHF and drawbead geometry. Both variables impose restrictions on sheet flow during stamping, and their interpolation determines the steel's performance in the operation. However, a more detailed explanation of the results is necessary. Therefore, a different model was sought for stamping test analysis, which would allow identifying the real effects of BHF and DB geometry on forming limit curve results.

For a more detailed analysis and a better understanding of the material's behavior during stamping, a study of the sheet metal mechanics during the forming process was conducted. This aimed to identify how the sheet deforms in certain regions along a specimen section. Figure 6 presents the defined regions in the specimen section, grouped along its profile.

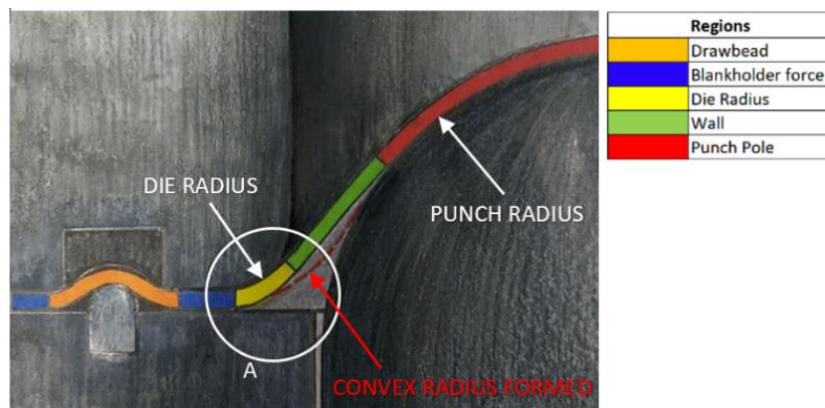


Figura 6 - Sheet metal mechanics during deformation.

In Figure 6, the blue regions represent the points where the blank holder force (BHF) acts directly on the material, between the flat surfaces of the die and the blank holder. The orange region represents the deformed area of the sheet at the bead profile, still within the flange. At the edge of the flange, in yellow, the bent region of the sheet at the die radius is shown, where the sheet is already flowing into the tooling. At this stage, when the material is subjected to the Bauschinger effect, the metal sheet curves counterclockwise (as indicated by the orientation in the figure). This phenomenon is known as "convex deformation" of the metal sheet. Studies by Gui et al. (2015) [45], David et al. (2021) [46], and Kim & Park (2020) [47] provide important insights into this behavior, highlighting its implications for material performance under cyclic loading conditions.

Beyond this point, the green region corresponds to the "wall" of the cup, and the red region to the punch pole. At the punch pole, the punch acts directly against the metal sheet, forming a pressure zone between the tooling and the material, under intense friction, where the sheet flows toward the wall region of the specimen - in the opposite direction to the sheet flow in the flange region, where it is pulled into the die. At the punch pole, the metal sheet also curves in the opposite direction to the curvature over the die radius, forming a "concave" profile on the material.

Based on these characteristics, it can be stated that the wall region, positioned between the die radius and the punch pole, is a friction-free zone, representing a critical transition in flow direction and sheet curvature during stamping. Given this, the mechanical behavior of the sheet in the wall region is directly affected by the restrictive force exerted on the sheet in the flange (defined by the blank holder force and bead geometry), which influences material flow and consequently the degree of strain hardening resulting from the sheet bending over the die radius.

The impact of the punch pole region on the wall region, affecting material flow in that direction, depends solely on the friction condition between the punch and the sheet, which remains constant in laboratory tests. In practical terms, additional variables must be considered beyond lubrication conditions, which affect the friction coefficient, such as tooling geometry (shape factor of the punch and die).

However, an observed characteristic in the stamped sheet sections was a third curvature along the specimen profile, located at the beginning of the wall region, near the die radius region (Figure 7). This curvature also exhibited a convex shape, similar to the curvature of the sheet over the die radius, and varied among the stamped specimens with different BHF and DB geometries. Although this curvature radius was not measured, its effect was evaluated based on deformation and microhardness measurements in the regions between the concentric circles.

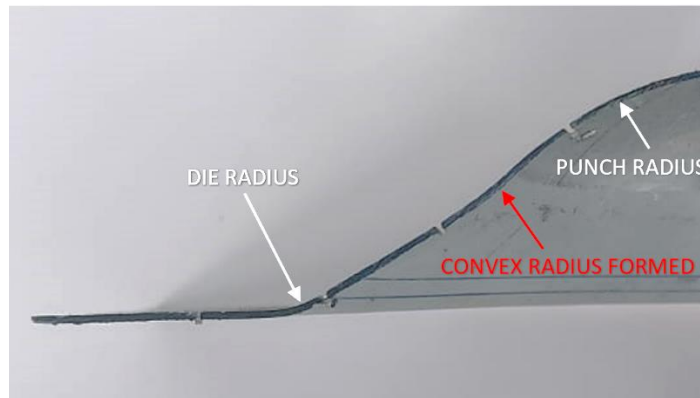


Figure 7 - Cross section of the specimen, with three radius formed by sheet metal strain.

Considering the mentioned aspects, it can be stated that the wall region of the sheet is directly impacted by the other regions of the specimen profile during stamping. Therefore, a more detailed analysis of these effects in this region can help explain the performance of DP600 steel through the forming limit curves. The resistive forces generated by the blank holder action were measured exclusively in the 200 × 200 mm specimens using a dynamometer. The tests were conducted with variations in BHF and different DB geometries, as shown in Figure 8.

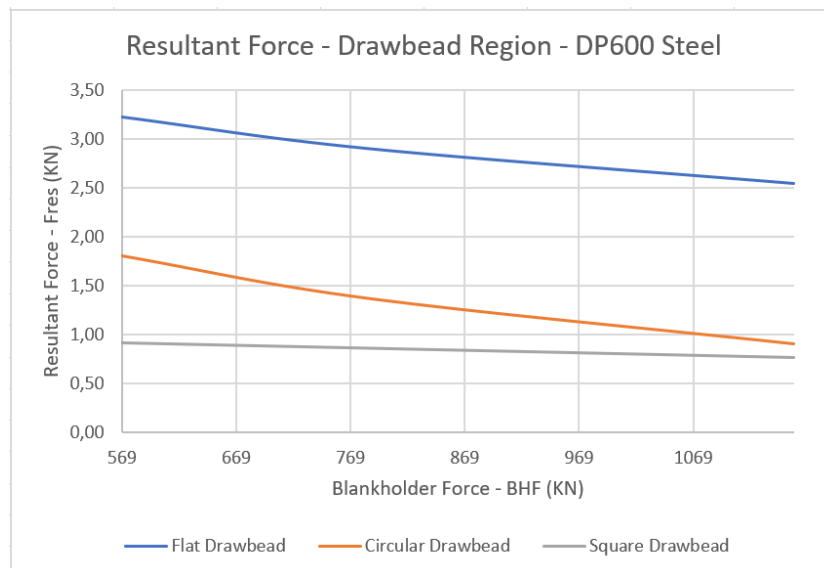


Figura 8 - Resultant forces on the sheet metal measured during the stamping tests.

According to the graph of the resultant force measured during the tests, the curves show a decrease in the resultant force with an increase in BHF. Considering that the resultant force stems from the movement of the sheet as it flows into the die, it is natural that with a lower BHF, the material advances further

during forming, leading to a higher resultant force (measured in terms of tensile load on the dynamometer shaft). For this reason, a drawbead (DB) geometry that creates greater restriction to sheet flow tends to present a lower resultant force curve compared to a DB geometry that offers less resistance to sheet flow.

Based on this, it is observed that the flat DB showed the highest values for resultant force, as it lacks a "tooth", meaning all resistive force is limited only to friction force, which varies based on different BHF values applied. Following this principle, when comparing DBs with circular and square geometries, it is noted that the square DB provides greater resistance to sheet flow than the circular DB.

The difference between the flat DB and the other geometry lies in the presence of the "tooth". Besides friction force, an additional force component is associated with the deformation of the sheet over the "tooth." These combined forces ($F_{at} + F_{db}$) define the resistive force (F_r) of each DB on sheet flow, where higher F_r results in lower resultant force (as measured by the dynamometer). Thus, for the same BHF value, the difference between the resistive force of the flat DB (without a "tooth") and the resistive forces of the toothed DBs (circular and square) corresponds to the resistive force of the drawbead, given that for the same BHF, the friction force component remains constant. This allows the calculation of the resistive force provided by the circular and square DBs for each BHF, subsequently determining the drawbead resistive force variation curve as a function of BHF for both geometries studied. As shown in Figure 9, a different behavior is observed between the circular and square DBs as BHF increases. For the circular DB, an increase in drawbead resistive force occurred with an increase in BHF, whereas for the square DB, the opposite trend was observed—the drawbead resistive force decreased as BHF increased. Considering the direct impact of forces acting on the flange on material flow and, consequently, on the deformation mode imposed on the sheet, this analysis is correlated with the difference in formability exhibited by the material through its forming limit curves (FLCs).

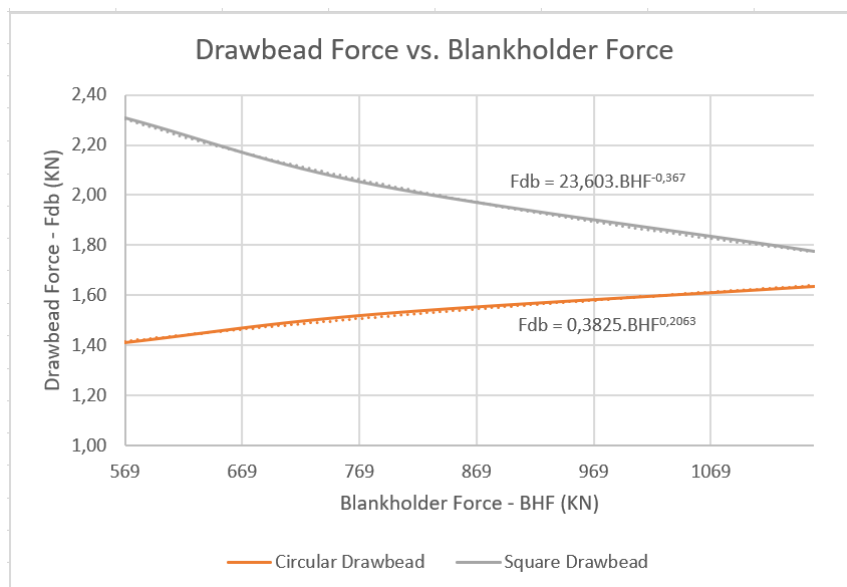


Figura 9 - Drawbead resistive forces of the circular and square drawbeads.

For the square DB, although the drawbead resistive force decreases with increasing BHF, it remains higher than the resistive force of the circular DB within the BHF range up to 1157 kN. It is observed that the resultant force for the square DB assumes an almost linear and nearly constant profile.

The fact that the resistive force of the square DB decreases with increasing BHF, while the resistive force of the circular DB increases with BHF, already characterizes the "shape effect" of the drawbead on resistive force in the flange. This means that a DB geometry that overly restricts sheet flow tends to lose effectiveness in the process as higher BHF values are applied, whereas a more uniform geometry, such as the circular DB, shows progressively greater efficiency as BHF increases.

In other words, two variables (DB and BHF) with similar functions—restricting sheet flow to balance flow during stamping—must "work together" (be directly proportional) to achieve greater efficiency in terms of sheet formability. When these variables tend to be inversely proportional, as in the square DB, there is a discrepancy in material flow control, leading to lower sheet stability. This effect is directly related to the hardness vs. deformation profile of the sheet at the beginning of the wall, where the critical zone (deformation instability) is most pronounced for the square DB. A more uniform deformation and hardness profile throughout the different regions of the stamped part, promoting a more homogeneous deformation condition and better formability, is achieved with the circular DB. Figure 10 shows the distribution of forces acting on the stamped specimen, providing a detailed illustration of load application along the stamped sheet.

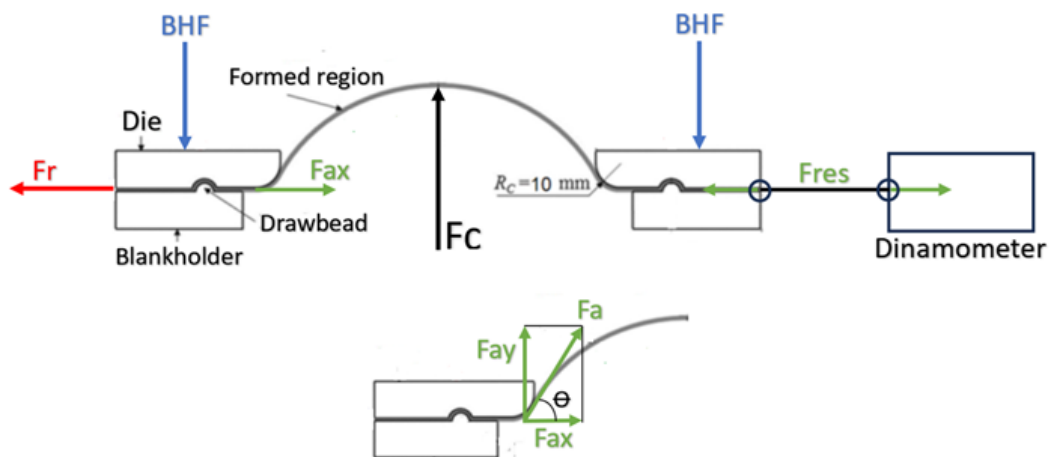


Figura 10 - Forces distribution on the stamped sheet metal.

Where:

- **Fa** = Active force resulting from the sheet forming force
- **Fax** = Active force component tangential to the blank holder surface
- **Fay** = Active force component perpendicular to the blank holder surface
- **Fr** = Resistive force
- **Fres** = Resultant force (measured by the dynamometer in the stamping test)
- **Fat** = Friction force
- **Fdb** = Drawbead force (resistive force the "tooth" provides to sheet flow)
- **Fc** = Forming force (measured by the FLC of the press)
- **BHF** = Blank holder force
- μ = Friction coefficient between the sheet and the tooling
- **Rc** = Radius of the entrance to the die cavity

The active force (F_a) acting on the sheet is generated by the force the punch exerts on the material during the forming process. The process begins with

the flat sheet (blank), which deforms into the die as the punch moves vertically. Thus, the angle Θ of the active force (F_a) varies from 0° , when the punch tangentially contacts the sheet, to a maximum value when material rupture occurs, for a given punch displacement (maximum drawing depth). The active force component (F_{ax}) is then defined by Equation (1):

$$F_{ax} = \frac{dF_a}{d\Theta} (1)$$

Considering the constant and normalized test speed, which does not imply a derivative of the equation with respect to time.

According to the figure, the active force component (F_{ax}) corresponds to the force with which the sheet is pulled horizontally over the flange into the die, as a result of the forming force (F_c) applied to stamp the material. During forming, a resistive force (F_r) acts in the flange against the sheet flow, arising from the sum of friction forces (F_{at}) and the force the drawbead exerts on material movement (F_{db}), given by Equation (2):

$$F_r = F_{at} + F_{db} (2)$$

In this equation, the friction force (F_{at}) can be determined as a function of the blank holder force (BHF), which acts in a direction normal to the blank holder surface, through Equation (3):

$$F_{at} = \mu \cdot BHF (3)$$

The resistive force provided by the drawbead (F_{db}), however, is difficult to determine due to the complexity of the stamping process, where a high number of variables influence the results. Therefore, using a device capable of measuring the sheet movement force during stamping becomes a more precise and efficient method for assessing the functional performance of the drawbead. Thus, a device was developed for measuring the tensile force exerted by the sheet during its flow, using a rod attached to the blank and a dynamometer, from which the resultant stamping force (F_{res}) was obtained. The measured resultant force (F_{res}) corresponds to the difference between the active force component (F_{ax}), which acts tangentially to the flange, and the total resistive force (F_r) in this region, given by Equation (4):

$$F_{res} = F_{ax} - F_r (4)$$

By substituting Equation (2) into Equation (4), we obtain:

$$F_{res} = F_{ax} - F_{at} - F_{db} (5)$$

For the flat drawbead, which does not have a "tooth," the resistive force of the drawbead (F_{db}) is zero, so Equation (5) can be rewritten as:

$$F_{ax} = F_{res} + F_{at} (6)$$

From this, the active force component (F_{ax}) can be easily determined. Thus, when performing stamping tests with flat, circular, and square DB geometries for the same blank holder force (BHF), the friction force becomes a constant in the equation. The difference obtained from measuring the resultant force (F_{res}) corresponds to the increment of the drawbead force (F_{db}) in Equation (5) when testing with circular and square DBs featuring a "tooth." Therefore, using the resultant force graph, the difference in F_{res} values between

the flat DB and the circular and square DBs corresponds to the Fdb values for these drawbeads, as provided in Table 3 and represented in Figure 9. This figure further defines the function representing the variation in drawbead resistive force according to the applied BHF.

Tabela 3 - Resistive force of the drawbead to the flow of the sheet.

FPC (KN)	Fdb (KN) Circular	Fdb (KN) Quadrado
569	1.41	2.31
785	1.52	2.04
1157	1.63	1.78

Further analyzing the decomposition of the active force (F_a) over the die radius, the component along the Y-axis (F_{ay}) is the force responsible for bending the sheet over the entrance edge of the die cavity (R_c). The radius of the entrance edge of the die cavity (R_c) is defined as the "shoulder radius of the die. Thus, in the stamping process, the sheet metal is bent over the "shoulder" radius of the die, with $R_c = 10$ mm, under the action of the force F_{ay} . The plastic deformation and resulting strain hardening imposed on the sheet during this bending define the Bauschinger effect in stamping operations, which can be evaluated based on the component F_{ay} of the active force (F_a).

4. CONCLUSIONS

The system was tested and is fully operational, proving to be efficient for measuring the restrictive force of sheet metal flow. Thus, it represents an important tool for evaluating sheet flow conditions based on blank holder force (BHF) and drawbead geometry, providing a more conclusive explanation of the effect of these variables on sheet formability.

The results of this study demonstrated the crucial influence of blank holder force (BHF) and drawbead geometry (DB) on the formability of DP600 steel. As expected, the forming limit curves (FLCs) revealed that both applied BHF and DB directly affect the material's formability. One of the most notable findings was the optimal stamping performance achieved with the circular drawbead and BHF of 1157 kN. In contrast, the worst performance occurred in tests using a flat drawbead, meaning without a tooth. This study proposed an analysis methodology using concentric circles printed on sample surfaces, which proved to be an effective analysis tool—this being the main conclusion of the research.

This model demonstrated, through deformation and hardness profiles of the stamped material, how the variables blank holder force and drawbead geometry affect the plastic behavior of steel during stamping across different deformation regions, conclusively explaining the results obtained via FLCs.

The work can show impact on stamping quality & industrial applications by analyzing deformation profiles in different material regions highlighted the importance of combining BHF and drawbead geometry to achieve more uniform deformations, which directly affects stamping quality. Thus, precise control based on advanced knowledge of these parameters is essential for optimizing stamping processes. Furthermore, analysis using concentric circles emphasized the importance of understanding the mechanical behavior of the material across different regions during the stamping process, enabling precise adjustments that

increase forming efficiency. In summary, beyond balancing material flow in the flange (brake), the drawbead also prevents the formation of dead zones, which harms formability and makes deformation more heterogeneous. The correlation between deformation variation and hardness led to defining functions representing the effect of BHF and drawbead geometry in the wall region of stamped specimens, which can be applied to numerical simulation models, improving their accuracy. Finally, the way the CCM (Concentric Circle Method) is applied in modified Nakazima stamping tests allows it to be replicated in practical industrial operations, by printing equidistant lines on blank surfaces, following the die and punch design.

5. REFERENCES

1. Keeler SP (1965) Determination of forming limits in automotive stampings. *Sheet Met Ind* 42:683–691
2. Goodwin GW (1968) Application os strain analyses to sheet metal forming problems in the press shop. *Metall Italiana* 60:764–774
3. Woodthorpe J, Pearce R (1969) The efect of r and n upon the forming limit diagrams of sheet metal. *Sheet Metal Ind* 1061–1067
4. ISO 12004–2 (2008) Metallic materials - sheet and strip - determination of forming-limit curve. European Committe for Standardization
5. SCHWINDT, Claudio D.; STOUT, Mike; IURMAN, Lucio; SIGNORELLI, Javier W.. Forming Limit Curve Determination of a DP-780 Steel Sheet. **Procedia Materials Science**, [S.L.], v. 8, p. 978-985, 2015. Elsevier BV. <http://dx.doi.org/10.1016/j.mspro.2015.04.159>.
6. PAUL, Surajit Kumar. Controlling factors of forming limit curve: a review. **Advances In Industrial And Manufacturing Engineering**, [S.L.], v. 2, p. 100033, maio 2021. Elsevier BV. <http://dx.doi.org/10.1016/j.aime.2021.100033>.
7. EMANUELA, Affronti; MARION, Merklein. Metallographic Analysis of Nakajima Tests for the Evaluation of the Failure Developments. **Procedia Engineering**, [S.L.], v. 183, p. 83-88, 2017. Elsevier BV. <http://dx.doi.org/10.1016/j.proeng.2017.04.015>.
8. LEONARD, Martín Eduardo; SIGNORELLI, Javier Walter; STOUT, Michael George; ROATTA, Analía. Métodos temporales para determinar deformaciones límite en chapas metálicas. **Matéria (Rio de Janeiro)**, [S.L.], v. 23, n. 2, p. 1-100, 19 jul. 2018. FapUNIFESP (SciELO). <http://dx.doi.org/10.1590/s1517-707620180002.0332>.
9. BELLONI, Valeria; RAVANELLI, Roberta; NASCETTI, Andrea; RITA, Martina di; MATTEI, Domitilla; CRESPI, Mattia. Py2DIC: a new free and open source software for displacement and strain measurements in the field of experimental mechanics. **Sensors**, [S.L.], v. 19, n. 18, p. 3832, 5 set. 2019. MDPI AG. <http://dx.doi.org/10.3390/s19183832>.
10. IQUILIO, R.A.; CERDA, F.M. Castro; MONSALVE, A.; GUZMÁN, C.F.; YANEZ, S.J.; PINA, J.C.; VERCRUYSSSE, F.; PETROV, R.H.; SAAVEDRA, E.I.. Novel experimental method to determine the limit strain by means of thickness variation. **International Journal Of Mechanical Sciences**, [S.L.], v. 153-154, p. 208-218, abr. 2019. Elsevier BV. <http://dx.doi.org/10.1016/j.ijmecsci.2019.01.036>.
11. GÓRSZCZYK, Jarosław; MALICKI, Konrad; ZYCH, Teresa. Application of Digital Image Correlation (DIC) Method for Road Material Testing. **Materials**, [S.L.], v. 12, n. 15, p. 2349, 24 jul. 2019. MDPI AG. <http://dx.doi.org/10.3390/ma12152349>.
12. BARLO, Alexander; SIGVANT, Mats; ENDEL, Benny. On the Failure Prediction of Dual-Phase Steel and Aluminium Alloys Exposed to Combined Tension and Bending. **Iop Conference Series: Materials Science and Engineering**, [S.L.], v. 651, n. 1, p. 012030, 1 nov. 2019. IOP Publishing. <http://dx.doi.org/10.1088/1757-899x/651/1/012030>.
13. HINO, Ryutaro; YASUHARA, Satoki; FUJII, Yutaka; HIRAHARA, Atsushi; YOSHIDA, Fusahito. Forming Limits of Several High-Strength Steel Sheets under Proportional/Non-Proportional Deformation Paths. **Advanced Materials Research**, [S.L.], v. 939, p. 260-265, 7 maio 2014. Trans Tech Publications, Ltd.. <http://dx.doi.org/10.4028/www.scientific.net/amr.939.260>.
14. PAN, Li Bo; ZHU, Hong Chuan; LEI, Ze Hong; ZHANG, Zhi Jian. Experimental Researches on Nonlinear Strain Paths Forming for Dual Phase Steel. **Advanced Materials Research**, [S.L.], v. 1004-1005, p. 209-213, 13 ago. 2014. Trans Tech Publications, Ltd.. <http://dx.doi.org/10.4028/www.scientific.net/amr.1004-1005.209>.
15. CARDOSO, Marcelo Costa; PEREIRA, Alexandre de Melo; SILVA, Fabiane Roberta Freitas da; MOREIRA, Luciano Pessanha. Experimental Analysis of Forming Limits and Thickness Strains of

DP600-800 Steels. **Applied Mechanics And Materials**, [S.L.], v. 835, p. 230-235, maio 2016. Trans Tech Publications, Ltd.. <http://dx.doi.org/10.4028/www.scientific.net/amm.835.230>.

16. FROHN-SÖRENSEN, Peter; NEBELING, Daniel; REUTER, Jonas; ENGEL, Bernd. A Critical Evaluation of Forming Limit Curves Regarding Layout of Bending Processes. **Key Engineering Materials**, [S.L.], v. 926, p. 1051-1060, 22 jul. 2022. Trans Tech Publications, Ltd.. <http://dx.doi.org/10.4028/p-d09adu>.
- [1] OLIVEIRA, Alex Raimundo de; LAJARIN, Sérgio Fernando; REBEYCA, Claudimir José; CHEMIN FILHO, Raviilson Antonio; NIKHARE, Chetan P.; MARCONDES, Paulo Victor Prestes. Influence of drawbead geometry and blank holder force on the dual phase steel formability. **The International Journal Of Advanced Manufacturing Technology**, [S.L.], v. 121, n. 9-10, p. 5823-5833, 19 jul. 2022. Springer Science and Business Media LLC. <http://dx.doi.org/10.1007/s00170-022-09603-4>.
17. SANRUTSADAKORN, Apichat; LAWONG, Winai; JULSRI, Weerapong. Numerical Study of Predicting Forming Process Based on Different Hardening Models in Advanced High Strength Steel Sheets. **Key Engineering Materials**, [S.L.], v. 951, p. 21-32, 7 ago. 2023. Trans Tech Publications, Ltd.. <http://dx.doi.org/10.4028/p-a0pkwh>.
18. REZAZADEH, V.; HOEFNAGELS, J.P.M.; GEERS, M.G.D.; PEERLINGS, R.H.J.. On the critical role of martensite hardening behavior in the paradox of local and global ductility in dual-phase steels. **European Journal Of Mechanics - A/Solids**, [S.L.], v. 104, p. 105152, mar. 2024. Elsevier BV. <http://dx.doi.org/10.1016/j.euromechsol.2023.105152>.
19. SHEN, Fu Hui; WANG, He Song; XU, Hao; LIU, Wen Qi; MÜNSTERMANN, Sebastian; LIAN, Jun He. Local Formability of Different Advanced High Strength Steels. **Key Engineering Materials**, [S.L.], v. 926, p. 917-925, 22 jul. 2022. Trans Tech Publications, Ltd.. <http://dx.doi.org/10.4028/p-dds916>.
20. PEREIRA, Rui; PEIXINHO, Nuno; COSTA, Sérgio L.. A Review of Sheet Metal Forming Evaluation of Advanced High-Strength Steels (AHSS). **Metals**, [S.L.], v. 14, n. 4, p. 394, 28 mar. 2024. MDPI AG. <http://dx.doi.org/10.3390/met14040394>.
21. KATIYAR, Lokendra Kumar. Enhancing mechanical properties and wear resistance of dual phase steel through surface mechanical attrition treatment. **Results In Surfaces And Interfaces**, [S.L.], v. 17, p. 100332, out. 2024. Elsevier BV. <http://dx.doi.org/10.1016/j.rsufi.2024.100332>.
22. PARK, Myeong-Heom; FUJIMURA, Yuto; SHIBATA, Akinobu; TSUJI, Nobuhiro. Effect of martensite hardness on mechanical properties and stress/strain-partitioning behavior in ferrite + martensite dual-phase steels. **Materials Science And Engineering: A**, [S.L.], v. 916, p. 147301, nov. 2024. Elsevier BV. <http://dx.doi.org/10.1016/j.msea.2024.147301>.
23. ABEYRATHNA, Buddhika; ROLFE, Bernard; HODGSON, Peter; WEISS, Matthias. A first step towards a simple in-line shape compensation routine for the roll forming of high strength steel. **International Journal Of Material Forming**, [S.L.], v. 9, n. 3, p. 423-434, 18 abr. 2015. Springer Science and Business Media LLC. <http://dx.doi.org/10.1007/s12289-015-1238-7>.
24. KE, Junyi; LIU, Yuqi; ZHU, Hongchuan; ZHANG, Zhibing. Formability of sheet metal flowing through drawbead – an experimental investigation. **Journal Of Materials Processing Technology**, [S.L.], v. 254, p. 283-293, abr. 2018. Elsevier BV. <http://dx.doi.org/10.1016/j.jmatprotec.2017.11.051>.
25. SCHMID, Harald; HETZ, Peter; MERKLEIN, Marion. Failure behavior of different sheet metals after passing a drawbead. **Procedia Manufacturing**, [S.L.], v. 34, p. 125-132, 2019. Elsevier BV. <http://dx.doi.org/10.1016/j.promfg.2019.06.129>.
26. SARAND, Mohammad Hasan Joudivand; MISIRLIOGLU, I. Burc. A physics-based plasticity study of the mechanism of inhomogeneous strain evolution in dual phase 600 steel. **International Journal Of Plasticity**, [S.L.], v. 174, p. 103918, mar. 2024. Elsevier BV. <http://dx.doi.org/10.1016/j.iijplas.2024.103918>.
27. KHAN, Muhammad Shehryar; SOLEIMANI, Maryam; MIDAWI, Abdelbaset R.H.; ADERIBIGBE, Isiaka; ZHOU, Y. Norman; BIRO, Elliot. A review on heat affected zone softening of dual-phase steels during laser welding. **Journal Of Manufacturing Processes**, [S.L.], v. 102, p. 663-684, set. 2023. Elsevier BV. <http://dx.doi.org/10.1016/j.jmapro.2023.07.059>.
28. RAJAK, Bijoy; KISHORE, Kaushal; MISHRA, Vipin. Investigation of a novel TIG-spot welding vis-à-vis resistance spot welding of dual-phase 590 (DP 590) steel: processing-microstructure-mechanical properties correlation. **Materials Chemistry And Physics**, [S.L.], v. 296, p. 127254, fev. 2023. Elsevier BV. <http://dx.doi.org/10.1016/j.matchemphys.2022.127254>.
29. CHENG, Nuo; YANG, Shanglei; LI, Yanlei; ZHAO, Xinlong; BI, Junhang; TIAN, Jiawei. Analysis of fatigue fracture mechanism of laser spiral welding of dissimilar metals of 6082 high strength aluminum alloy and DP980 high strength dual phase steel. **Materials Today Communications**, [S.L.], v. 41, p. 110665, dez. 2024. Elsevier BV. <http://dx.doi.org/10.1016/j.mtcomm.2024.110665>.
30. MANSUR, Vinicius Machado; MANSUR, Raquel Alvim de Figueiredo; CARVALHO, Sheila Medeiros de; SIQUEIRA, Rafael Humberto Mota de; LIMA, Milton Sergio Fernandes de. Effect of laser welding on microstructure and mechanical behaviour of dual phase 600 steel sheets. **Heliyon**, [S.L.], v. 7, n. 12, p. 1-100, dez. 2021. Elsevier BV. <http://dx.doi.org/10.1016/j.heliyon.2021.e08601>.

31. TIPALIN, Sergey A.; BELOUSOV, Vladislav B.; SHPUNKIN, Nikolay F.. Investigation of Uneven Properties of Stainless Steel 12Kh18N10T Depending on the Thickness of the Sheet. **Defect And Diffusion Forum**, [S.L.], v. 410, p. 28-36, 17 ago. 2021. Trans Tech Publications, Ltd.. <http://dx.doi.org/10.4028/www.scientific.net/ddf.410.28>.
- [2] ZHANG, Y.; DUAN, Y.; MU, Z.; FU, P.; ZHAO, J.. Non-Associated Flow Rule Constitutive Modeling Considering Anisotropic Hardening for the Forming Analysis of Orthotropic Sheet Metal. **Experimental Mechanics**, [S.L.], v. 64, n. 3, p. 305-323, 21 fev. 2024. Springer Science and Business Media LLC. <http://dx.doi.org/10.1007/s11340-024-01032-6>.
32. MENG, Bao; WAN, Min; WU, Xiangdong; YUAN, Sheng; XU, Xudong; LIU, Jie. Inner wrinkling control in hydrodynamic deep drawing of an irregular surface part using drawbeads. **Chinese Journal Of Aeronautics**, [S.L.], v. 27, n. 3, p. 697-707, jun. 2014. Elsevier BV. <http://dx.doi.org/10.1016/j.cja.2014.04.015>.
33. FOLLE, Luis Fernando; SCHAEFFER, Lirio. Avaliação das condições tribológicas em estampagem de chapas através do ensaio de dobramento sob tensão. **Matéria (Rio de Janeiro)**, [S.L.], v. 22, n. 2, p. 1-100, 2017. FapUNIFESP (SciELO). <http://dx.doi.org/10.1590/s1517-707620170002.0141>.
34. VOTAVA, Filip; JIRKOVÁ, Hana; KU?EROVÁ, Ludmila; JENÍ?EK, Št?pán. Study of Transition Areas in Press-Hardened Steels in a Combined Tool for Hot and Cold Forming. **Materials**, [S.L.], v. 16, n. 1, p. 442, 3 jan. 2023. MDPI AG. <http://dx.doi.org/10.3390/ma16010442>.
35. LIMA, Renan de Melo Correia; TOLOMELLI, Flávia Tereza dos Santos Fernandes; CLARKE, Amy J.; CLARKE, Kester D.; SPADOTTO, Julio Cesar; ASSUNÇÃO, Fernando Cosme Rizzo. Microstructural characterization of a 1100 MPa complex-phase steel. **Journal Of Materials Research And Technology**, [S.L.], v. 17, p. 184-191, mar. 2022. Elsevier BV. <http://dx.doi.org/10.1016/j.jmrt.2021.12.106>.
36. WEBBER, Eli; KNEZEVIC, Marko. Assessing strength of ferrite and martensite in five dual phase and two martensitic steels via high throughput nanoindentation to elucidate origins of strength. **Journal Of Materials Research And Technology**, [S.L.], v. 33, p. 3635-3648, nov. 2024. Elsevier BV. <http://dx.doi.org/10.1016/j.jmrt.2024.10.054>.
37. PEREIRA, A.F.G.; PRATES, P.A.; OLIVEIRA, M.C.; FERNANDES, J.V.. Inverse identification of the work hardening law from circular and elliptical bulge tests. **Journal Of Materials Processing Technology**, [S.L.], v. 279, p. 116573, maio 2020. Elsevier BV. <http://dx.doi.org/10.1016/j.jmatprotec.2019.116573>.
38. TRZEPIECINSKI, Tomasz. Recent Developments and Trends in Sheet Metal Forming. **Metals**, [S.L.], v. 10, n. 6, p. 779, 10 jun. 2020. MDPI AG. <http://dx.doi.org/10.3390/met10060779>.
39. LIMA, Tiago N.; CALLEGARI, Bruna; FOLLE, Luís Fernando; SANTOS, Ygor Tadeu B. dos; ZAMORANO, Luiz Gustavo; SILVA, Bruno Caetano dos S.; COELHO, Rodrigo Santiago. Microstructural Evolution of a Hot-Stamped Boron Steel Automotive Part and Its Influence on Corrosion Properties and Tempering Behavior. **Materials Research**, [S.L.], v. 26, p. 1-100, 2023. FapUNIFESP (SciELO). <http://dx.doi.org/10.1590/1980-5373-mr-2022-0494>.
40. NENE, Saurabh S.. Microstructure and Mechanical Properties of High Entropy Alloys. **High Entropy Alloys**, [S.L.], p. 99-175, 2024. Springer Nature Singapore. http://dx.doi.org/10.1007/978-981-99-7173-2_4.
41. **Artigo malha de círculo.**
42. CHEMIN FILHO, Ravilson Antonio; TIGRINHO, Luiz Mauricio Valente; BARRETO NETO, Rosalvo C; MARCONDES, Paulo Victor P. An experimental approach for blankholder force determination for DP600 with different material flow strain rates in the flange during stamping. **Proceedings Of The Institution Of Mechanical Engineers, Part B: Journal of Engineering Manufacture**, [S.L.], v. 227, n. 3, p. 417-422, 6 fev. 2013. SAGE Publications. <http://dx.doi.org/10.1177/0954405412471281>.
43. GUI, Hai-Lian; LI, Qiang; HUANG, Qing-Xue. The Influence of Bauschinger Effect in Straightening Process. **Mathematical Problems In Engineering**, [S.L.], v. 2015, p. 1-5, 2015. Hindawi Limited. <http://dx.doi.org/10.1155/2015/612840>.
44. DAVID, Felipe Farage; VASCONCELOS, Luan Marcel Costa; LIBERATO, Frank de Mello; COSTA, Adilson Rodrigues da. Academic production about the Bauschinger Effect in steels: a bibliometric study between 1990 and 2021. **I South Florida Congress Of Development**, [S.L.], p. 1-100, 10 jun. 2021. CONGRESS PROCEEDINGS I South Florida Congress of Development - 2021. <http://dx.doi.org/10.47172/sfcdv2021-0003>.
45. KIM, Hyung Lae; PARK, Sung Hyuk. Loading Direction Dependence of Yield-Point Phenomenon and Bauschinger Effect in API X70 Steel Sheet. **Metals And Materials International**, [S.L.], v. 26, n. 1, p. 14-24, 28 jun. 2019. Springer Science and Business Media LLC. <http://dx.doi.org/10.1007/s12540-019-00325-z>.